small NANO MICRO

Dielectrophoresis

DOI: 10.1002/smll.200701088

Microtubule Alignment and Manipulation Using AC Electrokinetics

*Maruti Uppalapati, Ying-Ming Huang, Thomas N. Jackson, and William O. Hancock**

The kinesin-microtubule system plays an important role in intracellular transport and is a model system for integrating biomotor-driven transport into microengineered devices. AC electrokinetics provides a novel tool for manipulating and organizing microtubules in solution, enabling new experimental geometries for investigating and controlling the interactions of microtubules and microtubule motors in vitro. By fabricating microelectrodes on glass substrates and generating AC electric fields across solutions of microtubules in low-ionic-strength buffers, bundles of microtubules are collected and aligned and the electrical properties of microtubules in solution are measured. The AC electric fields result in electro-osmotic flow, electrothermal flow, and dielectrophoresis of microtubules, which can be controlled by varying the solution conductivity, AC frequency, and electrode geometry. By mapping the solution conductivity and AC frequency over which positive dielectrophoresis occurs, the apparent conductivity of taxol-stabilized bovine-brain microtubules in PIPES buffer is measured to be 250 mS m^{-1}. By maximizing dielectrophoretic forces and minimizing electro-osmotic and electrothermal flow, microtubules are assembled into opposed asters. These experiments demonstrate that AC electrokinetics provides a powerful new tool for kinesin-driven transport applications and for investigating the role of microtubule motors in development and maintenance of the mitotic spindle.

Keywords:
- dielectrophoresis
- electrodes
- electro-osmotic flow
- microtubules
- molecular motors

1. Introduction

Microtubules are structurally polar cytoskeletal filaments that serve as tracks for kinesin and dynein motor proteins and provide mechanical integrity to the cell. In eukaryotic cells, kinesins use the energy of ATP hydrolysis to move unidirectionally along the microtubule surface, transporting intracellular cargo and driving the segregation of replicated chromosomes during cell division,[1] among other tasks. The components of the microtubule-kinesin motor system can be purified and motility reconstituted in vitro using the microtubule gliding assay[2] or bead assay.[3] Building on these in vitro assays, there has been considerable interest in exploiting this biologically derived nanoscale motion for manipulation, assembly and active transport of materials at the nanoscale.[4–7] However, to harness this biologically derived motion

[*] Prof. W. O. Hancock, M. Uppalapati[+]
Department of Bioengineering
229 Hallowell Bldg.
Penn State University
University Park, PA 16802 (USA)
E-mail: wohbio@engr.psu.edu
Prof. T. N. Jackson, Y.-M. Huang,[+]
Department of Electrical Engineering
216 Electrical Engineering West
Penn State University University
Park, PA 16802 (USA)

[+] These authors contributed equally to this work.

Supporting Information is available on the WWW under http://www.small-journal.com or from the author.

for such applications, it is necessary to develop tools to control microtubule-based motility. In addition, the development of in vitro techniques to harness these motors can also be used to manipulate microtubules into structures resembling the intracellular organization of microtubules, thereby providing tools for studying fundamental cellular processes such as axonal transport and mitosis.

Existing techniques for controlling microtubule motion on kinesin-coated surfaces include physical barriers and DC electric fields. Physical barriers such as microfabricated channels can guide the direction of microtubules driven by immobilized kinesin motors by buckling and redirecting the front end of moving microtubules.[8–12] We recently built on this work by creating fully enclosed microchannels functionalized with kinesin motors and generating high-density ensembles of uniformly oriented microtubules.[13] Electric fields can also be used to manipulate microtubules in vitro. In DC electric fields, microtubules undergo electrophoresis and move towards positive electrodes.[6,14,15] Precise electrophoretic control of kinesin-driven microtubule transport has been demonstrated using DC electric fields.[12,16] However, using DC electric fields in microchannels often results in electrophoresis of buffer ions, which poisons microtubule motility, and electrolysis that leads to bubble generation and electrode damage. Here, we characterize the behavior of microtubules in AC electric fields and show that AC electrokinetic phenomena can be used to organize microtubules into novel and useful assemblies in vitro.

In nonuniform AC electric fields, dielectrophoretic forces act on particles whose polarizability differs from that of the surrounding medium. If the particle is more polarizable than the surrounding medium, positive dielectrophoresis is observed, causing the particle to move towards regions of high field gradient.[17] Negative dielectrophoresis is observed when the particle is less polarizable than the surrounding medium, resulting in particle movement towards low-field-gradient regions. Dielectrophoresis of relatively large particles such as latex beads, cells, viruses, and bacteria has been reported.[18] However, significant electric-field gradients are required to manipulate particles as small as individual microtubules. Using lithography to fabricate microelectrodes on surfaces enables the generation of such field gradients but these high fields also generate electrohydrodynamic flows, which can potentially overpower the dielectrophoretic forces.[19] Dielectrophoresis has been used to manipulate macromolecules such as DNA,[20] actin filaments,[21] and microtubules[6] but the effect of electrohydrodynamic flows was not addressed in these studies. Moreover, we found that the dielectrophoresis of microtubules reported previously[6] depends strongly on small changes in experimental variables such as electrode geometry and buffer conditions. While electrorotation experiments on microtubules in uniform AC electric fields have been used to estimate electrical properties of microtubules,[14,22] there are no comprehensive studies using dielectrophoretic forces generated by nonuniform AC fields to manipulate, accumulate, and characterize the electrical properties of microtubules.

There have been reports of accumulations of latex particles, bacteria, yeast, and large DNA molecules in nonuniform AC electric fields that cannot be explained by dielectrophoretic forces alone.[23–26] Such accumulations have primarily been attributed to AC electro-osmotic flow.[25–27] At sufficiently low AC frequencies, an induced double layer of ions builds up on the electrode surfaces during each half-cycle. AC electro-osmotic flow results from the movement of these ions due to nonuniform electric fields tangential to the surface.[28] The other type of electrohydrodynamic flow generated by AC fields in conductive buffers is electrothermal flow. Electrothermal flow arises due to temperature gradients in the solution, which give rise to gradients in conductivity and permittivity. In the presence of an AC electric field, the conductivity and permittivity gradients produce body forces on the fluid that result in convective flows.[29] If dielectrophoretic forces are to be used to manipulate particles, then AC electro-osmotic and electrothermal flows must be minimized. However, when coupled with dielectrophoretic forces, these electrohydrodynamic flows can also be used to accumulate and concentrate particles on electrodes, and this phenomenon can in principle be used to accumulate microtubules.

Here we investigate the effects of buffer concentration, field strength and frequency, and electrode geometry on the behavior of microtubules in nonuniform AC fields. We identify optimal experimental conditions for minimizing electrohydrodynamic flows such that significant dielectrophoretic forces can be achieved and kinesin-driven microtubule motility is preserved. Furthermore, by characterizing the frequency and conductivity dependence of the positive dielectrophoretic forces, we estimate the conductivity of bovine-brain microtubules. Finally, we demonstrate that experimental conditions can be chosen to maximize AC electro-osmotic accumulation of high densities of microtubules. By choosing appropriate electrode geometries, this accumulation results in dense bundles of aligned (parallel and antiparallel) microtubules that can be used to investigate the role that motor proteins play in organizing microtubules into the mitotic spindle during cell division.

2. Results and Discussion

The goal of this work is to develop AC electrokinetics as a tool for manipulating microtubules in solution and organizing microtubules into aligned bundles on surfaces. The accumulation of microtubules on electrodes is described below, followed by an analysis of the roles played by AC electro-osmotic flow, electrothermal flow, and dielectrophoresis.

The first step of this work was to fabricate a pair of electrodes on a glass surface and observe the behavior of microtubules in solution when an AC voltage was applied. Chrome microelectrodes 15 μm wide and 12 mm long, separated by a gap of 20 μm, were patterned on glass substrates using conventional lithography techniques (Figure 1A). The substrates were then assembled into experimental chambers and rhodamine-labeled microtubules suspended in BRB16 buffer (16 mM PIPES, 1 mM $MgCl_2$, 1 mM EGTA, pH 6.9) were introduced. An AC voltage of 40 V_{p-p} was applied across the electrodes and the resulting microtubule behavior was observed by fluorescence microscopy. At frequencies above

NANO MICRO small

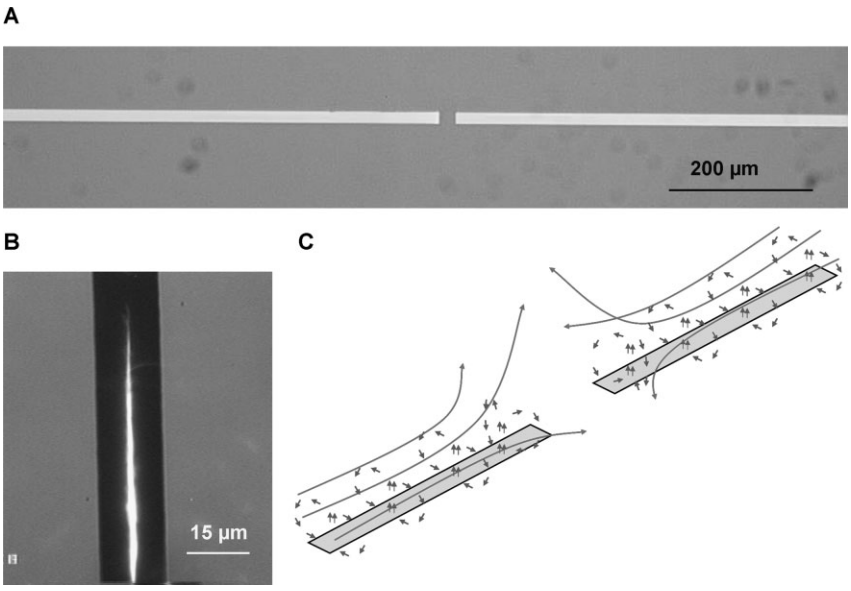

Figure 1. Electrode design and AC-field-driven microtubule accumulation. A) Optical micrograph of Cr electrodes 15 μm wide and 12 mm long, separated by a gap of 20 μm. B) Accumulation of microtubules resulting from application of 40 V_{p-p} at 500 kHz across the electrodes. C) Schematic of electrohydrodynamic flows leading to microtubule accumulation. Small arrows denote electro-osmotic flow and large arrows denote electrothermal flow. The accumulation and flows can also be seen in Supporting Information Movies 1 and 2.

500 kHz, bulk solution flow was observed along the electrodes, with the dominant flow being directed inward towards the gap separating the electrode pair. At 500 kHz and below, dense bundles of microtubules accumulated along the centerline of the electrodes as far as 400 μm away from the gap separating the electrodes (see Figure 1B and Supporting Information Movie 1). Upon closer inspection, there were two distinct flow patterns (as shown in Figure 1C and Supporting Information Movie 2). The first flow pattern occurred in the solution roughly 7 μm above the electrodes and was directed towards the electrode gap, while the second flow pattern occurred at the electrode surface and formed vortices perpendicular to the long axis of the electrodes. These electrohydrodynamic flows continued indefinitely as long as the AC voltage across the electrodes was maintained, and they stopped instantly when the field was switched off. We next set out to understand the origin of these flow patterns.

2.1. AC Electro-osmotic Flow

AC electro-osmotic flow occurs in nonuniform fields at low frequencies where tangential electric fields act on the induced double layer of ions on the electrode surface.[28] The ion movement due to Coulomb forces creates a drag on the bulk fluid that results in electro-osmotic flow. The mechanism of AC electro-osmosis is illustrated in Figure 2. In the half-cycle shown in Figure 2A, a positive potential is applied to the right electrode and a negative potential to the left electrode. This results in the accumulation of negatively charged ions on the right electrode and positive ions on the left electrode. Due to the action of tangential-electric-field components, the Coulomb forces on the double layer are always pointed toward the electrode edges, irrespective of the polarity of the electrodes, and have maximal amplitude closest to the gap separating the two electrodes. This results in symmetric flow on both electrodes with ions moving away from the gap (Figure 2B). The velocity of fluid flow is given by:[28]

$$v = \frac{E_t \sigma_q}{\kappa \eta} \quad (1)$$

where E_t is the tangential component of electric field, σ_q is the surface charge density in the diffuse double layer, κ is the reciprocal Debye length, and η is the solution viscosity. In AC fields, both the induced charge as well as the potential drop across the solution are frequency dependent. At low frequencies, there is capacitive charging of the double layer and the potential drop is mainly across the double layer, resulting in E_t tending to zero. At high frequencies, the ions can not move fast enough to form a double layer during each half-cycle; therefore σ_q tends to zero. Hence, the strongest electro-osmotic flow is achieved at intermediate frequencies.[28]

A flow pattern was observed, consisting of vortices near the electrode edges oriented perpendicular to the long axis of the electrodes (Figure 1C). This flow disappeared at high frequencies, consistent with electro-osmotic flow.[28] Because the direction of electro-osmotic flow is determined by the direction of the tangential electric field at the electrode surface, we used finite-element modeling to simulate the tangential electric fields surrounding each electrode. The simulated tangential field lines at a plane 0.5 μm above the electrode surface are shown in Figure 2C. Except for regions of the electrodes closest to the gap, the field direction along most of the length of each electrode is perpendicular to the long edge of the electrode. Hence, during each half-cycle, counterions moving to the electrode surface to form the double layer create inward flow from the edge that meets at the centerline of the electrode and rise upward, setting up vortices. As discussed below, the microtubule accumulations along the electrodes (i.e., Figure 1B) primarily result from this inward AC electro-osmotic flow.

2.2. Electrothermal flow

Electrothermal flow results from temperature gradients in the solution, which give rise to gradients in the solution conductivity and permittivity. Temperature gradients can be generated from external sources or through Joule heating[30] but a major mechanism for generating the temperature gradients that drive electrothermal flow has been found to be illumination from the light source of the microscope, which leads to absorptive heating of the electrodes.[30,31] To understand and quantify electrothermal flow in our system, we carried out simulations and performed experiments using

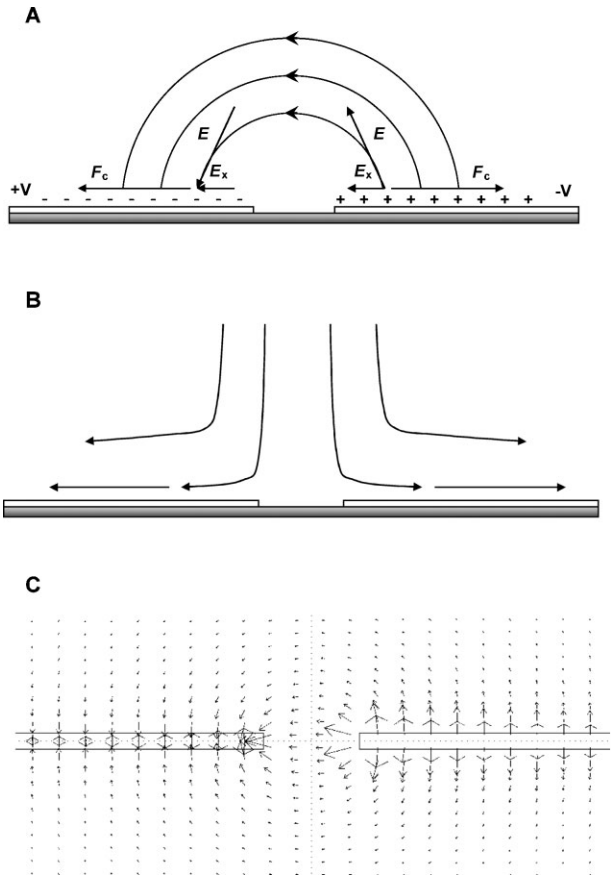

Figure 2. Mechanism of AC electro-osmotic flow. A) During each half cycle, counter ions accumulate on each electrode. Tangential electric-field components (E_x) lead to Coulombic forces (F_c) that are directed away from the gap, irrespective of the electrode polarity. B) The resulting ion fluxes cause electro-osmotic fluid flow away from the electrode gap. C) Using the same electrode geometry as in the experiments, a simulation of the tangential components of the electric field in the *x*–*y* plane just above the surface. The resulting ion flow results in inward fluid flow towards the center of the electrodes from all edges.

tracer particles to map the electrothermal flow. The body force on a fluid in terms of permittivity and conductivity gradients is given by[29]

$$\langle f_e \rangle = \frac{1}{2}\mathrm{Re}\left[\frac{\sigma\varepsilon(\alpha-\beta)}{\sigma+i\omega\varepsilon}(\nabla T\cdot E)E-\frac{1}{2}\varepsilon\alpha|E|^2\nabla T\right] \quad (2)$$

$$\alpha=\left(\frac{1}{\varepsilon}\right)\left(\frac{\partial\varepsilon}{\partial T}\right) \quad \beta=\left(\frac{1}{\sigma}\right)\left(\frac{\partial\sigma}{\partial T}\right)$$

where σ is the conductivity and ε the permittivity of the solution, T is the temperature, E is the applied electric field, and Re denotes the real component of the complex number. The first term on the right-hand side, which dominates at low frequencies, represents Coulomb forces due to the space charge density generated by the conductivity and permittivity gradients. The second term on the right-hand side, which dominates at high frequencies, represents dielectric forces. For the electrode geometries used here, the temperature gradient and therefore the permittivity and conductivity gradients are expected to be uniform along the length of the electrodes. However, the field strength is highest near the gap separating the electrodes. Previous work using similar electrode geometries showed that temperature gradients lead to inward bulk fluid flow along each electrode that converges at the electrode gap to create vertical flow normal to the surface at the electrode gap.[30,31]

To model the expected electrothermal flow profile for our electrode geometry, we carried out finite element simulations using a pair of electrodes separated by a 20-μm gap. The electrode temperatures were set to 10 °C above ambient to simulate electrode heating from the microscope illumination, and a 35 V_{p-p}, 1.5 MHz AC voltage was applied across them. As seen from the streamlines in Figure 3A, the simulation predicted inward flow along the electrode surfaces that converged to a vertical flow in the electrode gap, with a return path in solution. To characterize the speed and direction of electrothermal flow in our experimental chambers, the movement of 1-μm fluorescent polystyrene beads in solution was quantified at different illumination intensities. One test of whether observed flows are electrothermal in nature is to reduce the microscope illumination (reducing the associated heating of the electrodes) and test whether flow velocities are diminished. In the 100-μm-thick experimental chamber, the bottom surface contained a pair of 15-μm-wide electrodes separated by a 20-μm gap, similar to Figure 1A. A 30 V_{p-p}, 500 kHz AC voltage was applied across the electrodes and the bead movements observed by fluorescence microscopy. As seen in Figure 3B and C, and in Supporting Information Movie 3, at a height of ≈7 μm above the surface, the beads moved parallel to the electrodes toward the gap and flow velocities fell with increasing distance away from the electrodes. These flow trajectories are similar to the electrothermal flow observed by others (see Figure 3 in Reference [30]) and qualitatively agree with our simulations. As expected for electrothermal flow, when neutral density filters were used to reduce the illumination of the 100 W mercury arc lamp on the microscope by a factor of 64, there was an 85% decrease in the flow velocity of tracer particles. When the electric field was switched off while maintaining constant illumination, the flow stopped immediately, demonstrating that the flows are not due to simple convection. Hence, we conclude that the inward-directed bulk flows observed along the electrodes were electrothermal in origin and that the temperature gradients driving this flow were primarily due to heating of the electrodes by microscope illumination.

2.3. Microtubule Accumulation Due to Electrohydrodynamic Flow

One behavior that we consistently observed at frequencies below 500 kHz was the accumulation of microtubules along the centerline of the two electrodes up to hundreds of micrometers away from the electrode gap. At these frequencies, microtubules did not accumulate near the electrode gap (Figure 1B) and, interestingly, microtubules could be observed moving away from the electrode gap (Supporting Information Movie 1). This behavior has not been documented using this electrode geometry or with particles having aspect ratios

small NANO MICRO

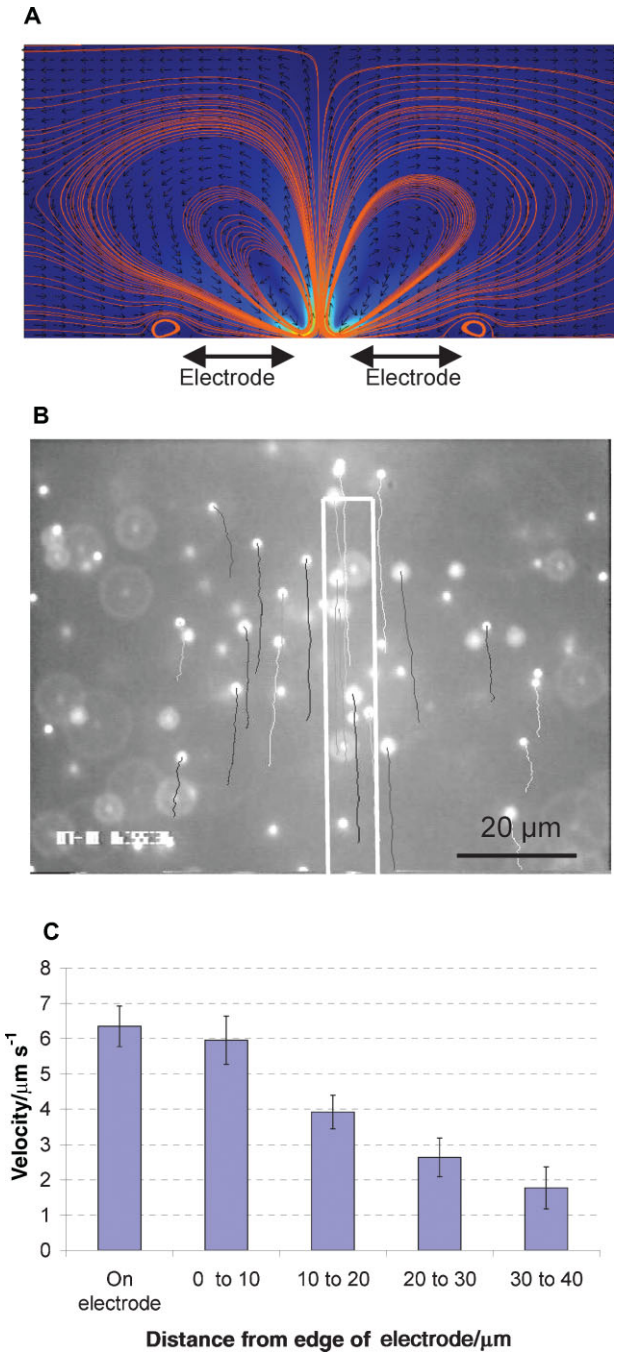

Figure 3. Simulation and experimental observation of electrothermal flow resulting from microscope illumination. A) Simulation of electrothermal flow, showing the flow vectors above two 100-μm-long electrodes separated by a 20-μm gap (side view). Note that near the electrode surface, flow is observed towards the gap. B) Experimental flow profiles (top view) observed by tracking fluorescent beads at a height of ≈7 μm above the electrode surface. The traces show the track taken by each particle in the 5 s preceding the image. For clarity, only one electrode is shown and every bead is observed to move toward the gap separating the electrodes. C) Particle velocities along a line perpendicular to the electrode at a distance of 50 μm from the gap. Velocities are maximal directly above the electrode and fall of with increasing lateral distances away from the electrode edge.

approaching microtubules, and for biological experiments this phenomenon could provide a model for the microtubule organization in neurons or a geometry to test the sorting of mixed orientation filaments by molecular motors. As described below, we believe that this accumulation is driven by electro-osmotic flow that sweeps the microtubules into the center of the electrode, and that dielectrophoretic forces that attract microtubules to the electrode edges may also be playing a role.

As seen in Figure 2C, away from the electrode gaps the electric-field vector parallel to the surface is directed perpendicular to the electrode axis and is strongest at the edges of the electrodes. This field distribution sets up electro-osmotic flow that, at the surface, is directed toward the center of the electrode, and that converges to a stagnation point at the centerline and flows upwards into solution from there. The result of this flow is a pair of vortices (see Figure 1C and Supporting Information 2) with an energy minimum at the centerline, where the flow velocity is zero and shear forces are balanced. Microtubules oriented parallel to the electrodes accumulate at the centerline of the electrodes, and any filaments not precisely aligned are swept away by the vortex flow.

One argument for electro-osmotic flow being the driver for microtubule accumulation is that the degree of accumulation correlates with the predicted and observed magnitude and direction of electro-osmotic flow. At the electrode surface, the calculated tangential electric field (Figure 2C) falls with increasing distance away from the electrode gap and the rate of electro-osmotic flow, as observed by following fluorescent beads or microtubules in solution, similarly fell at distances away from the electrode gap. The fact that microtubules accumulated at these positions of maximal electro-osmotic flow suggests a mechanism in which a minimum organizing flow rate is necessary to overcome Brownian motion of the microtubules in solution. As seen in Figure 4, the region over which microtubules accumulate depends strongly on the AC excitation frequency. At frequencies above 500 kHz there was no accumulation but at lower frequencies the accumulation zone grew and the accumulation start point moved farther away from the gap. At 50 kHz, the microtubule accumulation zone began 15 μm from the electrode gap and continued for over 400 μm. Because at lower frequencies there is more time during each half-cycle to accumulate the ion double layer (see Equation (1)), electro-osmotic flow is expected to be larger at lower frequencies, and qualitative observations supported this. Because the tangential electric field is strongest directly adjacent to the electrode gap (Figure 2C) and because the electro-osmotic flow is predicted and observed to be directed *away* from the electrode gap in this region, the fact that the microtubule accumulation begins farther from the gap and extends for a longer distance at lower frequencies is consistent with electro-osmotic flow driving the microtubule accumulation.

In previous AC electrokinetics experiments, the accumulation of latex particles observed by others has been attributed to a combination of AC electro-osmotic flow and positive dielectrophoretic forces. For instance, using large electrodes so that only a single vortex is formed on each electrode (in contrast to the pairs of vortices in our experiments), Green and Morgan[32] and Hoettges et al.[25] found that positive

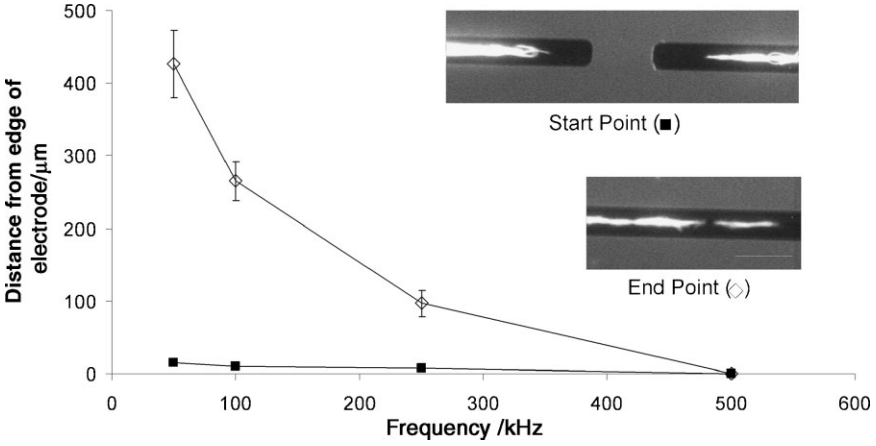

Figure 4. Frequency dependence of microtubule accumulation. Electrodes are 10 μm wide and separated by a 20-μm gap. BRB12 buffer was used with 40 V_{p-p} field stimulation. Insets show the start points and end point of the accumulation zone (scale bar 20 μm). Distances are measured from the edge of each electrode and are displayed as mean ± standard deviation from 4 to 6 determinations for each point.

dielectrophoretic forces attract particles towards the electrode edges, while electro-osmotic flow pushes the particles away from the edges. These opposing forces lead to particles accumulating at a stagnation point whose position is frequency dependent. A recent study that used AC electrokinetics to accumulate viruses on surface electrodes also concluded that, while positive dielectrophoresis plays a role, the drag forces generated by electrohydrodynamic flows are the main driving force for accumulation.[33]

While AC electro-osmotic flow appears to be the dominant mechanism for microtubule accumulation in our experiments, there is strong evidence that dielectrophoresis also plays an important role. First, the densities of microtubules observed on the electrodes are difficult to explain without attractive dielectrophoretic forces playing a role. Second, in buffers above 16 mM PIPES where electro-osmotic flow is evident but no dielectrophoresis is seen, microtubules do not accumulate on the electrodes. Third, under some conditions two bands of microtubules were observed on the electrodes (data not shown), consistent with a balance between dielectrophoretic forces directed toward the electrode edges and electro-osmotic flow directed toward the electrode midline. However, because dielectrophoresis is expected to be negligible at distances far from the electrode gap, accumulations of microtubules observed hundreds of micrometers away from the electrode gaps (Figure 4) must be predominantly driven by electro-osmotic forces. It is possible that these microtubules are collected on the electrodes closer to the gap and migrate long distances along the electrodes by outward electro-osmotic flow.

2.4. Microtubule Dielectrophoresis

To develop dielectrophoresis as a tool for manipulating microtubules and to characterize the electrical properties of microtubules, we identified experimental conditions where dielectrophoresis dominates and quantified the dielectrophoretic forces on microtubules. When a 30 V_{p-p}, 5 MHz AC potential difference was applied across a pair of castellated electrodes, which are routinely used in dielectrophoresis studies because they have clearly defined regions at their tips where electric-field gradients are maximized, microtubules accumulated at the high-field-gradient regions, indicating positive dielectrophoresis (Figure 5). Others have observed similar accumulations of actin filaments in AC fields.[34] One difficulty in characterizing dielectrophoresis is that electrohydrodynamic flow can overwhelm the dielectrophoretic forces.[19] Using the paired electrodes shown in Figure 1, we systematically analyzed the dependence of microtubule dielectrophoresis on the AC frequency and buffer conductivity. As discussed above, at low frequencies AC electro-osmotic flow away from the electrode gap plays a dominant role, while at high frequencies electrothermal flow towards the gap dominates. We characterized this in more detail by observing the microtubule accumulation at the tips of the opposed electrodes (the region of highest electric-field gradient) as a function of frequency in BRB12 buffer (Figure 6). At frequencies from 100 kHz to 1 MHz (Figure 6A–D), microtubules are attracted to the electrode tips by dielectrophoresis but are pushed away from the gap by AC electro-osmotic flow. In contrast, at 2.5 MHz, electro-osmotic flow is balanced by electrothermal flow directed toward the gap, and dielectrophoresis dominates (Figure 6E). Above roughly 7 MHz, electrothermal flow towards the electrode gap dominates. Hence, there is a range of frequencies centered around 5 MHz where electro-osmotic and electrothermal flows are balanced, providing a window where dielectrophoretic forces on microtubules can be analyzed.

In a conducting medium, particles that have a different polarizability than the medium are attracted to regions of high field gradient. The dielectrophoretic force on a particle is given by[35]

$$\langle F_{\mathrm{DEP}} \rangle = \frac{1}{4} \nu \mathrm{Re}[\tilde{\alpha}] \nabla |E|^2 \qquad (3)$$

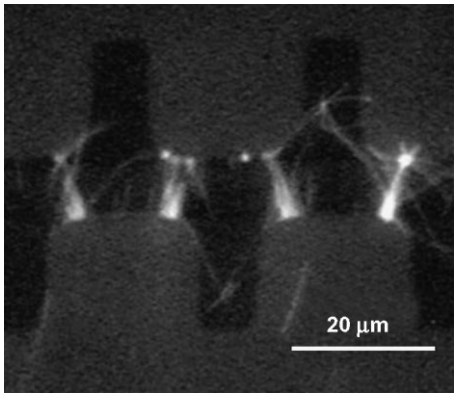

Figure 5. Positive dielectrophoresis of microtubules using castellated electrodes at 5 MHz frequency and 35 V_{p-p} amplitude in BRB3 buffer.

small NANO MICRO

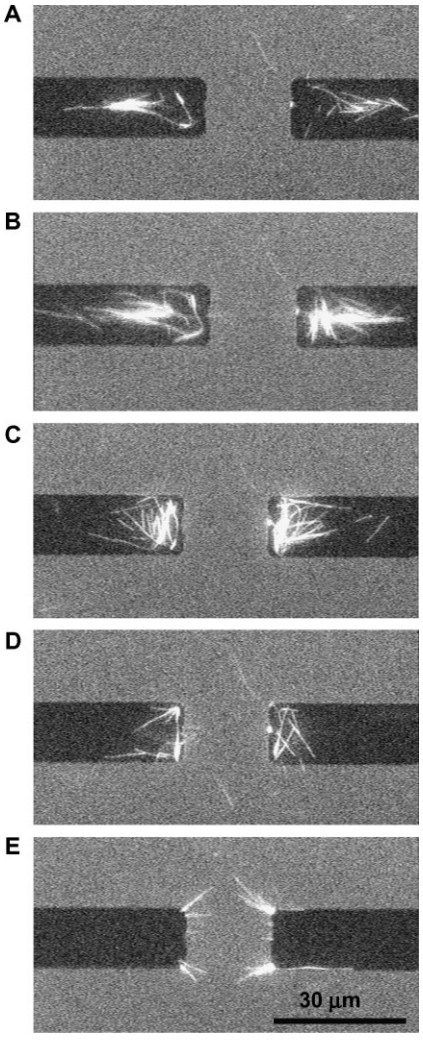

Figure 6. The dependence of microtubule accumulation on AC frequency using opposed electrodes. At high frequencies, dielectrophoresis dominates, while at lower frequencies, electro-osmotic flows push the microtubules away from the electrode gap. Experiments were performed in BRB12 buffer with 30 V_{p-p} stimulation. Frequencies were A) 100 kHz, B) 250 kHz, C) 500 kHz, D) 1 MHz, and E) 2.5 MHz.

where $\mathrm{Re}[\tilde{\alpha}]$ is the real part of the effective polarizability of the particle (also called the Claussius-Mossotti factor), E is the electric field, and ν is the volume of the particle. Microtubules can be considered as prolate ellipsoids with their major axis $\gg$ minor axes. The effective polarizability of a prolate ellipsoid along the major axis when the major axis aligns with the electric field is given by Morgan and Green[35] as:

$$\tilde{\alpha} = \varepsilon_m \frac{\tilde{\varepsilon}_p - \tilde{\varepsilon}_m}{\tilde{\varepsilon}_m} \tag{4}$$

where $\tilde{\varepsilon}_p$ and $\tilde{\varepsilon}_m$are the complex permittivities of the particle and the medium, respectively. These complex permittivities are given by:

$$\tilde{\varepsilon}_m = \varepsilon_m - \frac{i\sigma_m}{\omega}, \quad \tilde{\varepsilon}_p = \varepsilon_p - \frac{i\sigma_p}{\omega} \tag{5}$$

where ε_p, σ_p, ε_m and σ_m are the permittivity and conductivity of the particle and the medium, respectively. Equations (3–5) can be combined to obtain a relationship for the dielectrophoretic force as a function of the conductivities and permittivities of the particle and the medium:

$$\langle F_{DEP} \rangle = \frac{1}{4} \nu \varepsilon_m \left[\frac{\omega^2 \varepsilon_m (\varepsilon_p - \varepsilon_m) + \sigma_m (\sigma_p - \sigma_m)}{\omega^2 \varepsilon_m^2 + \sigma_m^2} \right] \nabla |E|^2 \tag{6}$$

In the 5 MHz range where electrohydrodynamic flows are minimal, the dielectrophoretic forces from Equation (6) are dominated by conductivity differences between the microtubule and the buffer; only at much higher frequencies are permittivity differences expected to play a role. Consistent with this, greater accumulations of microtubules were seen in lower-ionic-strength buffers than in high-ionic-strength buffers (data not shown). One implication of this simplification is that the effective conductivity of microtubules can be estimated by finding the solution conductivity at which dielectrophoretic forces disappear (i.e., σ_p–σ_m). This zero-force approach was used by Hughes et al. to obtain an estimate of 100 mS m^{-1} for the internal conductivity of Herpes Simplex Virus type-I particles.[36] Using identical electrodes to Figure 6 and a frequency of 2.5 MHz, we measured the accumulation of microtubules as a function of buffer conductivity. Robust microtubule accumulation was clearly observed in BRB6 and BRB12 buffers, very few microtubules accumulated at the electrode tips in BRB16 buffer, and no microtubule accumulation was observed in BRB20 buffer. Assuming that microtubule accumulation is due to dielectrophoretic forces, this puts the apparent conductivity of microtubules very close to the conductivity of our BRB16 buffer, which we measured to be 250 mS m^{-1} (see Experimental Section). Because the apparent microtubule conductivity is dominated by the ion double layer surrounding this negatively charged polymer, this value holds for the buffers used in these experiments and is expected to vary with buffer composition. This microtubule conductivity value is roughly twofold higher than the 120 mS m^{-1} measured by Minoura and Muto using microtubule electrorotation experiments.[22] In that work, the buffer consisted of 1 mM MES plus 10 μM $MgCl_2$.

2.5. Estimating Dielectrophoretic Forces on Microtubules

By using estimates for the microtubule and buffer permittivities and conductivities and by calculating the square of the electric-field gradient ($\nabla|E|^2$), it is possible to use Equation (6) to calculate the magnitude of the dielectrophoretic forces on microtubules in our experiments. In Figure 7A, finite-element modeling was used to calculate the spatial distribution of both the electric field E and the square of the electric-field gradient, $\nabla|E|^2$. The simulations used an electrode geometry identical to Figure 6 (15-μm-wide electrodes separated by a 20-μm gap) with 35 V applied across the electrodes in BRB6 buffer. The maximum $\nabla|E|^2$ occurs near the edges of the electrodes and falls steeply with distance away from the edges, which qualitatively agrees with the

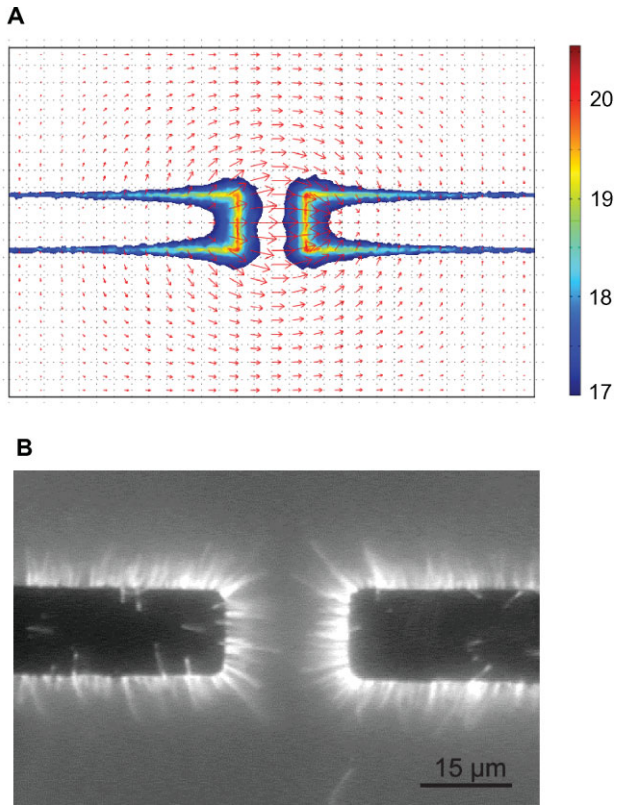

Figure 7. Dielectrophoresis of microtubules. A) Simulation of the electric field and electric-field gradients using opposed electrodes. Simulations used 35 V_{p-p} amplitude in BRB6 buffer. Red arrows denote the electric-field vectors and colors denote $\nabla|E|^2$. To better visualize the data, values are scaled logarithmically and gradients less than $10^{17}\,V^2\,m^{-3}$ are not shown. B) Dielectrophoretic accumulation of microtubules at electrode edges agree with the simulations (AC voltage of 35 V_{p-p}, 5 MHz in BRB6 buffer).

microtubule accumulations observed in Figure 6E. Using the microtubule and buffer conductivities ($250\,mS\,m^{-1}$ and $116\,mS\,m^{-1}$, respectively), the known dimensions of microtubules (25-nm diameter), the calculated maximal $\nabla|E|^2$ ($\approx 10^{-20}\,V^2\,m^{-3}$, Figure 7), and reported relative permittivity of microtubules (1 to 100[22]), we estimated the dielectrophoretic forces on microtubules in our experiments. At a frequency of 5 MHz in BRB6 buffer, the maximal dielectrophoretic force per unit length of microtubule was estimated to be $\approx 10\,pN\,\mu m^{-1}$. Varying the microtubule permittivity from 1 to 100 changed this value by less than 5% at 5 MHz, demonstrating that dielectrophoresis of microtubules is dominated by conductivity differences and not permittivity differences between microtubules and the bufffer in which they are suspended. It should also be noted that calculating the overall force on a microtubule requires integration over the entire length of the microtubule, and that these maximum forces are localized to the electrode edges. Nonetheless, as shown in Figures 5 and 6, these forces are sufficient to attract and align microtubules between the electrodes. Furthermore, previous work using DC electric fields and magnetic fields showed that forces on the order of 1–5 $pN\,\mu m^{-1}$ are sufficient to redirect microtubules being transported along kinesin-functionalized surfaces.[12,37]

2.6. Kinesin Motility in Low-Ionic-Strength-Buffers

Having identified buffer ionic strengths and AC frequencies over which positive dielectrophoresis can be used to manipulate microtubules, it is important for future work on kinesin-driven microtubule transport to ensure that kinesin motors retain their function under these same conditions. To test whether kinesin functionality is retained in these low-ionic-strength buffers, microtubule gliding experiments were carried out in BRB12, BRB6, and BRB3 at pH 7.0. We found that in BRB12 and BRB6, microtubules moved for 30 and 6 minutes, respectively, before depolymerizing but in BRB3 microtubules depolymerized within one minute. An antifade system is used in these experiments to scavenge dissolved oxygen from solution and thus prevent the formation of fluorophore-induced oxygen free radicals that bleach fluorophores and damage proteins. The end product of this reaction is gluconic acid, which leads to a decrease in the solution pH over time. Therefore, as the molarity of the buffer decreases, the buffering capacity is diminished, resulting in earlier loss of motility. In order to circumvent this problem, solutions were degassed prior to use and the flow chambers were sealed with vacuum grease to block atmospheric oxygen from dissolving in the buffers. Additionally, in order to allow some working room before sealing the flow cell, the initial pH of the low-molarity buffers was increased (see Experimental Section) to compensate for the initial production of gluconic acid. By following this protocol, we were able to extend the lifetime of motility in all three low-ionic-strength buffers to greater than three hours. Hence, in future experiments it should be possible to use dielectrophoresis to manipulate microtubules driven by immobilized kinesin motors.

2.7. Mimicking Cellular Organization of Microtubules

The chief motivation for developing novel approaches for manipulating microtubules in solution is to establish new in vitro assays for investigating the role of microtubules and molecular motors in mitosis and other fundamental biological processes. Elegant experiments using gene targeting to inhibit specific kinesin motors in dividing cells have identified putative roles for different motors in building and maintaining the mitotic spindle.[38,39] Complementing these cellular studies, experiments using purified motor proteins and microtubules in vitro have demonstrated that complex assemblies such as asters and vortices can be generated from a very simple parts list of biological components.[40,41] To better understand the role of microtubule dynamics and molecular motors in mitotic-spindle assembly and chromosome transport, new experimental strategies are needed that enable manipulation of microtubules into spindle-like assemblies in a geometry that permits the analysis of motor behavior by fluorescence microscopy. From Figure 6, it was shown that electrokinetic flows are minimized at 5 MHz, enabling dielectrophoretic forces to play a dominant role. Further, the simulation in Figure 7A predicts strong dielectrophoretic forces on microtubules using paired electrodes at 5 MHz in BRB6 buffer. Using this identical geometry, buffer conductivity, and AC voltage, this prediction was confirmed

NANO MICRO small

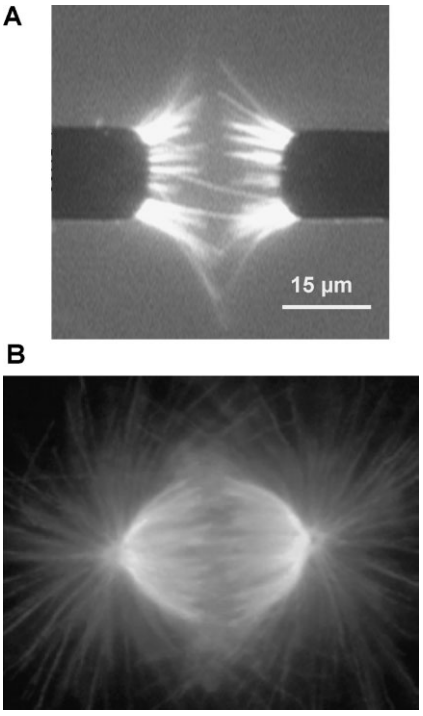

Figure 8. Spindle-like accumulation of microtubules. A) Opposed microtubule asters generated by dielectrophoretic accumulation of microtubules at electrode edges. AC voltage of 35 V_{p-p}, 5 MHz was applied across the electrodes and microtubules were suspended in BRB12 buffer. B) For comparison, a static immunofluorescence image of a dividing cell at metaphase. Typical pole–pole distances in cells are 12–15 μm. Image adapted from Wittmann et al., [45] reproduced with permission from Macmillan Publishers Ltd, copyright 2001.

in Figure 7B. A 35 V_{p-p} potential across the electrodes resulted in microtubules being pulled out of solution onto the edges of the electrodes, the regions of highest field gradient. By using a slightly higher ionic-strength buffer, BRB12, microtubules accumulated solely at the tips of the electrodes (Figure 8A), analogous to the opposed asters of microtubules that make up the mitotic spindle in dividing cells (Figure 8B). This result is a first step towards building artificial mitotic spindles for studying, in a controlled in vitro setting, the complex interactions of motors and microtubules that underlie cell division. For these experiments to better mimic an actual spindle, the microtubules need to be sorted from their mixed polarity found here to uniform polarity with their plus ends overlapping and the minus ends, which are normally organized by the centrosome, would need to be bundled or somehow fixed in place. These are areas of ongoing work in our lab. Nonetheless, this result shows the potential for using AC electrokinetic manipulation of microtubules to investigate fundamental questions in cell biology.

3. Conclusion

Because microelectrodes can be fabricated on glass surfaces with virtually any geometry, AC electrokinetics has the potential to be a powerful tool for manipulating microtubules in experimental work or for applications integrating biomotors and microtubules into microengineered devices. We found that when solutions of taxol-stabilized microtubules are subjected to AC electric fields, three AC electrokinetic phenomena become apparent: electro-osmotic flow, electrothermal flow, and dielectrophoresis. Interestingly, along long (12 mm) narrow (10–20 μm) electrodes, the electro-osmotic and electrothermal flow results in dense bundles of microtubules aligning along the long axis of the electrodes. This result has implications in transport applications where microtubules can be concentrated from solution or for studying kinesin motility along bundles of microtubules similar to the axon, provided that subpopulations of parallel and antiparallel oriented microtubules can be sorted out. These aligned bundles of mixed orientation microtubules are also a convenient model to test the organizing activities of tetrameric Eg5 and other mitotic motors. Finally, by minimizing the electrohydrodynamic flows, we identified conditions in which pN-scale dielectrophoretic forces on microtubules can be achieved. These experiments lay the foundation for applying AC electrokinetics as a tool for studying the role of molecular motors in mitotic-spindle function and for guiding microtubules in motor-driven transport applications.

4. Experimental Section

Microtubules and kinesin: Tubulin was purified from bovine brain[42] and labeled with rhodamine,[43] as previously described. Microtubules were polymerized by mixing 32 μM rhodamine-labeled tubulin, 4 mM $MgCl_2$, 1 mM GTP, and 5% DMSO in BRB80 buffer (80 mM piperazine-1,4-bis(2-ethanesulfonic acid) (PIPES), 1 mM ethylene glycol-bis(2-aminoethylether)-*N*,*N*,*N*′,*N*′-tetraacetic acid (EGTA), 1 mM $MgCl_2$, pH 6.9 with KOH), incubating at 37 °C for 20 min, and then diluting into a solution containing 10 μM paclitaxel. The microtubules were pelleted using a Beckman Airfuge at 30 psi and were resuspended in BRB3, BRB6, BRB12, BRB16, and BRB20 buffers (3 mM, 6 mM, 12 mM, 16 mM and 20 mM PIPES, respectively, with 1 mM EGTA and 1 mM $MgCl_2$). Buffer conductivities were measured using an AKTA FPLC system (Amersham Biosciences) and found to vary linearly with increasing PIPES concentration. The linear fit for the conductivity as a function of PIPES concentration was σ_{buffer} (mS m^{-1}) = 11.4 × [PIPES (mM)] + 48.0.

The nominal pH of these buffers was 7.0 but for some experiments the pH of the low-molarity buffers was raised, as noted in the text. Antifade reagents (20 mM D-glucose, 0.02 mg mL^{-1} glucose oxidase, 0.008 mg mL^{-1} catalase and 70 mM β-mercaptoethanol) were added to the buffer and the microtubules were observed using epifluorescence microscopy (Nikon E600, 60× 1.2 NA water-immersion objective). Fluorescent microtubules were visualized using a Genwac GW-902H CCD camera and recorded to videotape. Frames were digitized using Scion Image (Scion Corporation) and image analysis carried out using Image. In some experiments, 1-μm-diameter poly(styrene) beads (Bang Laboratories) labeled with rhodamine were added to the microtubule solution as tracer particles to determine flow velocities.

Full-length *Drosophila* conventional kinesin was bacterially expressed and purified using previously published protocols.[44]

Electrode fabrication and application of AC electric fields: To generate AC electric fields in our microchambers, Cr microelectrodes were patterned on glass and these surfaces assembled into flow chambers. Masks used for photolithography were fabricated using a Mann 3600 pattern generator. Before electrode fabrication, glass substrates were cleaned by immersion in acetone and isopropyl alcohol in an ultrasonic bath for 10 minutes each, followed by immersion in piranha solution (H_2SO_4:H_2O_2 = 4:1) for 20 minutes. The piranha treatment both cleans the glass and results in a high-surface-energy OH-saturated surface that improves the adhesion of deposited layers. To pattern electrodes, a 100-nm Cr layer was deposited onto the cleaned glass surface using an Edward E306A sputtering system. Shipley 1811 photoresist was then spun on top of the Cr layer and this photoresist was patterned through the photomask using a Karl Suss MA-55 aligner. The exposed photoresist and underlying Cr were removed by wet etching and the remaining unexposed photoresist dissolved by acetone to expose the patterned electrodes.

Flow chambers were assembled on the electrode-patterned glass substrates using a coverslip and 3M double-sided tape as spacers. The surfaces were blocked with casein (0.5 mg m L^{-1} casein in BRB80) and then flushed with 64 nM microtubules and 0.2 mg L^{-1} casein in appropriate buffer containing antifade reagents. The leads of the electrodes were connected to a function generator (BK precision, Yorba Linda, CA, USA) and AC electric fields with frequencies varying from 10 kHz to 10 MHz were applied with a maximum peak–peak voltage of 40 V. At low frequencies, Faradaic charging of the electrodes occurs due electrochemical reactions at the electrode surface, which can affect the electro-osmotic flow.[26] Since such reactions often damage the electrodes, in the present work we avoided frequencies below 10 kHz.

Motility in low-molarity buffers: To study kinesin function in low-molarity buffers, flow cells were prepared with Fisher's Finest glass slides and Corning 18-mm coverglass, using 3M double-sided tape as spacers. The flow cells were incubated with 0.5 mg mL^{-1} casein for 5 min, flushed with a motor solution containing 5 μg mL^{-1} kinesin, 0.2 mg mL^{-1} casein, and 1 mM ATP, and incubated for 5 min. Motility solution (64 nM microtubules, 10 μM paclitaxel, 20 mM D-glucose, 0.02 mg L^{-1} glucose oxidase, 0.008 mg mL^{-1} catalase, and 0.07 M β-mercaptoethanol) was then introduced into the flow cell and microtubule movement was visualized. Initial experiments used BRB3, BRB6, and BRB12 all at pH 7.0. For additional experiments the pH values of BRB12, BRB6, and BRB3 were increased to 7.5, 8.0, and 9.0, respectively, and the buffers were degassed.

Finite-element-model simulations: Because AC electrokinetics is a complex phenomenon involving a combination of dielectrophoretic forces and electro-osmotic and electrothermal fluid flow, we used finite-element modeling using the COMSOL Multiphysics package to predict and understand the observed phenomena. To predict the direction of electro-osmotic flow, the tangential electric fields surrounding each electrode were simulated using COMSOL Multiphysics in the 3D conductivity mode. The model consisted of two electrodes 0.1 μm high, 10 μm wide, and 400 μm long, separated by a gap of 20 μm. The left electrode was set to +5 V and the right electrode set to −5 V, the solution conductivity was set to 0.170 S m^{-1}, and the solution permittivity set to 78.5.

To model the predicted electrothermal flow, the Electrostatics, Convection, and Conduction, and Incompressible Navier-Stokes application modes were used in a 2D simulation. The flow chamber in the simulation was 400 μm wide and 200 μm high, and the electrodes were placed on the bottom surface with zero thickness and an electrode gap of 20 μm. Equation (2) was used to calculate body forces due to Joule heating and electrode heating from illumination was modeled by setting the temperature of the electrodes to 10 °C above the surrounding environment. The simulation used a 40 V_{p-p} 1.5 MHz AC potential across the electrodes, a fluid conductivity of 0.116 S m^{-1} (BRB6 buffer), a dynamic viscosity of 0.006 kg m^{-1} s^{-1} for the fluid, and an initial fluid velocity of zero.

For calculating dielectrophoretic forces, the Electric Currents mode was used to calculate the spatial distribution of both the electric field E and the square of the electric-field gradient, $\nabla|E|^2$ in a simulated chamber 100 μm by 150 μm with a height of 10 μm. The simulation modeled a pair of 15-μm-wide electrodes separated by a 20-μm gap, with 35 V_{p-p} applied across the electrodes in BRB6 buffer.

Acknowledgements

This project was funded by the Penn State Center for Nanoscale Science (NSF MRSEC DMR0213623) and by an NSF Biophotonics Grant (0323024) to W.O.H. and T.N.J. funded jointly by NSF and NIH/NIBIB.

[1] N. Hirokawa, Y. Noda, Y. Okada, *Curr. Opin. Cell Biol.* **1998**, *10*, 60.
[2] J. Howard, A. J. Hudspeth, R. D. Vale, *Nature* **1989**, *342*, 154.
[3] S. M. Block, L. S. Goldstein, B. J. Schnapp, *Nature* **1990**, *348*, 348.
[4] H. Hess, *Science* **2006**, *312*, 860.
[5] H. Hess, V. Vogel, *J. Biotechnol.* **2001**, *82*, 67.
[6] L. Jia, S. G. Moorjani, T. N. Jackson, W. O. Hancock, *Biomed. Microdevices* **2004**, *6*, 67.
[7] L. Limberis, J. Magda, R. Stewart, *Nano Lett.* **2001**, *1*, 277.
[8] L. Cheng, M. Kao, E. Meyhöfer, L. Guo, *Small* **2005**, *1*, 409.
[9] J. Clemmens, H. Hess, R. Doot, C. M. Matzke, G. D. Bachand, V. Vogel, *Lab Chip* **2004**, *4*, 83.
[10] Y. Hiratsuka, T. Tada, K. Oiwa, T. Kanayama, T. Q. Uyeda, *Biophys J.* **2001**, *81*, 1555.
[11] S. Moorjani, L. Jia, T. Jackson, W. Hancock, *Nano Lett.* **2003**, *3*, 633.
[12] M. G. L. van den Heuvel, M. P. de Graaff, C. Dekker, *Science* **2006**, *312*, 910.
[13] Y.-M. Huang, M. Uppalapati, W. O. Hancock, T. N. Jackson, *Biomed. Microdevices* **2007**, *9*, 175.
[14] K. J. Böhm, N. E. Mavromatos, A. Michette, R. Stracke, E. Unger, *Electromagn. Biol. Med.* **2005**, *24*, 319.
[15] M. van den Heuvel, C. Butcher, S. Lemay, S. Diez, C. Dekker, *Nano Lett.* **2005**, *5*, 235.
[16] T. Kim, M. T. Kao, E. F. Hasselbrink, E. Meyhofer, *Nano Lett.* **2007**, *7*, 211.

[17] H. A. Pohl, *Dielectrophoresis: The Behavior of Neutral Matter in Nonuniform Electric Fields*, Cambridge University Press, Cambridge, UK **1978**.
[18] C. F. Gonzalez, V. T. Remcho, *Sep. Sci.* **2005**, *1079*, 59.
[19] A. Castellanos, A. Ramos, A. Gonzalez, N. G. Green, H. Morgan, *J. Phys. D: Appl. Phys.* **2003**, *36*, 2584.
[20] C. L. Asbury, A. H. Diercks, G. van den Engh, *Electrophoresis* **2002**, *23*, 2658.
[21] S. B. Asokan, L. Jawerth, R. L. Carroll, R. E. Cheney, S. Washburn, R. Superfine, *Nano Lett.* **2003**, *3*, 431.
[22] I. Minoura, E. Muto, *Biophys. J.* **2006**, *90*, 3739.
[23] M. R. Bown, C. D. Meinhart, *Microfluid. Nanofluid.* **2006**, *2*, 513.
[24] N. G. Green, A. Ramos, H. Morgan, *J. Phys. D: Appl. Phys.* **2000**, *33*, 632.
[25] K. F. Hoettges, M. B. McDonnell, M. P. Hughes, *J. Phys. D: Appl. Phys.* **2003**, *36*, L101.
[26] J. Wu, Y. Ben, D. Battigelli, H. C. Chang, *Ind. Eng. Chem. Res.* **2005**, *44*, 2815.
[27] K. H. Bhatt, S. Grego, O. D. Velev, *Langmuir* **2005**, *21*, 6603.
[28] A. Ramos, H. Morgan, N. G. Green, A. Castellanos, *J. Colloid Interface Sci.* **1999**, *217*, 420.
[29] A. Ramos, H. Morgan, N. G. Green, A. Castellanos, *J. Phys. D: Appl. Phys.* **1998**, *31*, 2338.
[30] N. G. Green, A. Ramos, A. Gonzalez, A. Castellanos, H. Morgan, *J. Electrostatics* **2001**, *53*, 71.
[31] N. G. Green, A. Ramos, A. Gonzales, A. Castellanos, H. Morgan, *J. Phys. D: Appl. Phys.* **2000**, *33*, L13.
[32] N. G. Green, H. Morgan, *J. Phys. D: Appl. Phys.* **1998**, *31*, L25.
[33] A. Docoslis, L. A. Espinoza, B. Zhang, L. L. Cheng, B. A. Israel, P. Alexandridis, N. L. Abbott, *Langmuir* **2007**, *23*, 3840.
[34] M. E. Arsenault, H. Zhao, P. K. Purohit, Y. Goldman, H. H. Bau, *Biophys. J.* **2007**, *93*, L42.
[35] H. Morgan, N. G. Green, in *Microtechnologies and Microsystems Series 2, AC Electrokinetics: Colloids and Nanoparticles* (Ed: R. Pethig), Research Studies Press, Baldock **2003**, p. 41.
[36] M. P. Hughes, H. Morgan, F. J. Rixon, *Biochim. Biophys. Acta* **2002**, *1571*, 1.
[37] B. M. Hutchins, M. Platt, W. O. Hancock, M. E. Williams, *Small* **2007**, *3*, 126.
[38] G. Goshima, F. Nedelec, R. D. Vale, *J. Cell Biol.* **2005**, *171*, 229.
[39] C. Zhu, J. Zhao, M. Bibikova, J. D. Leverson, E. Bossy-Wetzel, J. B. Fan, R. T. Abraham, W. Jiang, *Mol. Biol. Cell* **2005**, *16*, 3187.
[40] F. J. Nedelec, T. Surrey, A. C. Maggs, S. Leibler, *Nature* **1997**, *389*, 305.
[41] T. Surrey, F. Nedelec, S. Leibler, E. Karsenti, *Science* **2001**, *292*, 1167.
[42] R. C. Williams, Jr., J. C. Lee, *Methods Enzymol.* **1982**, *85*, 376.
[43] A. Hyman, D. Drechsel, D. Kellogg, S. Salser, K. Sawin, P. Steffen, L. Wordeman, T. Mitchison, *Methods Enzymol.* **1991**, *196*, 478.
[44] W. O. Hancock, J. Howard, *J. Cell Biol.* **1998**, *140*, 1395.
[45] T. Wittmann, A. Hyman, A. Desai, *Nat. Cell Biol.* **2001**, *3*, E28.

Received: November 8, 2007
Revised: March 3, 2008

